Systematic Strategies for Stochastic Mode Reduction in Climate

ANDREW J. MAJDA

Courant Institute of Mathematical Sciences, Center for Atmosphere–Ocean Science, New York University, New York, New York

ILYA TIMOFEYEV* AND ERIC VANDEN-EIJNDEN

Courant Institute of Mathematical Sciences, New York University, New York, New York

(Manuscript received 16 July 2002, in final form 9 January 2003)

ABSTRACT

A systematic strategy for stochastic mode reduction is applied here to three prototype ''toy'' models with nonlinear behavior mimicking several features of low-frequency variability in the extratropical atmosphere. Two of the models involve explicit stable periodic orbits and multiple equilibria in the projected nonlinear climate dynamics. The systematic strategy has two steps: stochastic consistency and stochastic mode elimination. Both aspects of the mode reduction strategy are tested in an a priori fashion in the paper. In all three models the stochastic mode elimination procedure applies in a quantitative fashion for moderately large values of $\varepsilon \approx 0.5$ or even $\varepsilon \approx 1$, where the parameter ε roughly measures the ratio of correlation times of unresolved variables to resolved climate variables, even though the procedure is only justified mathematically for $\varepsilon \ll 1$. The results developed here provide some new perspectives on both the role of stable nonlinear structures in projected nonlinear climate dynamics and the regression fitting strategies for stochastic climate modeling. In one example, a deterministic system with 102 degrees of freedom has an explicit stable periodic orbit for the projected climate dynamics in two variables; however, the complete deterministic system has instead a probability density function with two large isolated peaks on the ''ghost'' of this periodic orbit, and correlation functions that only weakly ''shadow'' this periodic orbit. Furthermore, all of these features are predicted in a quantitative fashion by the reduced stochastic model in two variables derived from the systematic theory; this reduced model has multiplicative noise and augmented nonlinearity. In a second deterministic model with 101 degrees of freedom, it is established that stable multiple equilibria in the projected climate dynamics can be either relevant or completely irrelevant in the actual dynamics for the climate variable depending on the strength of nonlinearity and the coupling to the unresolved variables. Furthermore, all this behavior is predicted in a quantitative fashion by a reduced nonlinear stochastic model for a single climate variable with additive noise, which is derived from the systematic mode reduction procedure. Finally, the systematic mode reduction strategy is applied in an idealized context to the stochastic modeling of the effect of mountain torque on the angular momentum budget. Surprisingly, the strategy yields a nonlinear stochastic equation for the large-scale fluctuations, and numerical simulations confirm significantly improved predicted correlation functions from this model compared with a standard linear model with damping and white noise forcing.

1. Introduction

The climate system has a wide range of timescales for important physical processes. Thus on hourly scales there are boundary layer and small-scale convective processes; on daily scales there are organized synoptic-scale weather events; on monthly scales there is low-frequency variability of the extratropics and intraseasonal variability of the Tropics (Ghil and Robertson 2002); on annual scales there is the El Niño–Southern Oscillation and midlatitude planetary teleconnections (Trenberth et al. 1998); finally, on decadal scales there are important oscillations of the coupled midlatitude atmosphere–ocean system (Griffies and Bryan 1997). For example, in this last case, a reduced description of the atmosphere is needed in studying patterns of coupled decadal variability such as the North Atlantic oscillation. There is an obvious need in such a complex system for systematic and rigorous strategies for reducing the number of degrees of freedom while retaining fidelity of important features of the unresolved variables. Such reductive strategies help to develop deeper physical un-

* Current affiliation: Department of Mathematics, University of Houston, Houston, Texas.

Corresponding author address: Prof. Andrew J. Majda, Courant Institute of Mathematical Sciences, 251 Mercer Street, New York, NY 10012.
E-mail: jonjon@cims.nyu.edu

derstanding of the various components of the climate system and their interaction. They also provide useful reduced mathematical models that are much more computationally efficient. Hasselmann (1976) proposed the idea of simplified stochastic modeling for the unresolved degrees of freedom in climate dynamics with important contributions by Leith (1975).

In recent years, stochastic modeling of the extratropical atmosphere has been an active research topic (Branstator 1995; DelSole and Farrel 1996; Selten 1997; Newman et al. 1997; Branstator and Haupt 1998; Whitaker and Sardeshmukh 1998; Achatz and Brantstator 1999), including stochastic modeling for the angular momentum budget (Weickmann et al. 2000; Egger 2001; Egger and Hoinka 2002). For example, as regards low-frequency variability of the extratropical atmosphere, Brantstator (1995) and Whitaker and Sardeshmukh (1998) have developed reduced linear stochastic models through regression fitting of linear Langevin dynamics, which assumes a structure with white noise forcing and linear damping. For the angular momentum budget, regression fitting of interesting phenomenological linear Langevin models (Weickmann et al. 2000) and higher-order Markov models (Egger 2001; Egger and Hoinka 2002) have been utilized.

A different approach to understanding low-frequency variability of the atmosphere through the nonlinear dynamics and bifurcation theory of a reduced number of suitable climate variables has been developed beginning with the seminal work of Charney and DeVore (1979). This approach involves identifying structures such as multiple equilibria or stable periodic orbits in the phase space of reduced nonlinear climate variables (Legras and Ghil 1985; Jin and Ghil 1990; Ghil and Robertson 2002) and then utilizing the observational record or global circulation models to search for the ''ghost'' of this behavior in the full complex dynamics with many degrees of freedom (Marcus et al. 1994, 1996; Itoh and Kimoto 1996). In this context, explicit stochastic models involving Markov jump processes have been utilized to mimic random jumps between different basins of low-frequency variability in observations (Vautard and Legras 1988; Kimoto and Ghil 1993). Also, the effects of small random additive noise have been analyzed in a similar fashion (DeSwart and Grasman 1987) when introduced in an ad hoc fashion in the simplest scenario for multiple equilibria (Charney and DeVore 1979).

The work mentioned in the previous paragraph requires regression fitting of an assumed linear stochastic model to the observed climate and its fluctuations. By necessity this approach to stochastic modeling has severe limitations for predicting climate change and diagnosing its causes. Alternative systematic a priori stochastic mode reduction strategies are needed for more practical prediction and improved regression fitting. This is the main focus of the present paper, which is based on a systematic mathematical strategy for stochastic mode reduction developed recently by the authors (Majda et al. 1999, 2001, hereafter called MTV-1 and MTV-2). The stochastic-mode reduction techniques (MTV-1; MTV-2) is a two-step procedure based on the assumption that the degrees of freedom under consideration have been split into essential resolved modes whose dynamics is the main objective and unessential unresolved modes, which are to be eliminated in the reduced description. In the first step of the procedure, the equations of motion for the unresolved modes are modified by representing the nonlinear self-interaction terms between unresolved modes by stochastic terms. The motivation is that the self-interaction terms are responsible for the sensitive dependence on small perturbations in the system on short timescales, and that these modes can indeed be represented by stochastic terms if coarse-grained modeling on longer timescales, as for climate, is the objective. This step in the procedure is *stochastic consistency.* In the second step of the procedure, the equations of motion for the unresolved modes are then eliminated using standard projection technique for stochastic differential equations (Khasminsky 1963; Gardiner 1985; MTV-1; MTV-2). The elimination step is mathematically rigorous in the limit where the stochastic terms are infinitely fast, corresponding to the situation where the unresolved modes evolve much faster than the resolved ones. This step is *stochastic mode elimination.*

This systematic mode reduction technique has two obvious advantages. First, the ad hoc simplification of the original dynamics is made on the level of the unresolved modes rather than the resolved ones. This is unlike the procedures described in the second paragraph above that are in common use in the atmospheric science community where the approximations are developed on the resolved modes, one drops all couplings with the unresolved modes, and replaces them by ad hoc stochastic terms of linear Langevin type, with parameters obtained by regression fitting. In contrast, the systematic mode reduction procedure predicts the structure of the stochastic terms in the equations for the resolved modes (MTV-1; MTV-2) and this structure can be surprisingly rich: nonlinear corrections arise, multiplicative noises occur, both stable and unstable linear Langevin terms arise, or all in combination, depending on the quantitative features of the underlying dynamics (MTV-2). The second advantage of the technique is its rigor in an appropriate limiting parameters range, which can be deduced a priori from the original equations. This provides a guideline for the applicability of the method, which is an important feature of the procedure.

The goals of the work presented here are (i) to demonstrate how nonlinear dynamics on a reduced set of resolved climate variables can be modified significantly by the interaction with unresolved modes, (ii) to utilize the systematic mode reduction strategy (MTV-1; MTV-2) to predict the detailed structure of the stochastic dynamics resulting from this interaction, and (iii) to compare these predictions with the results from resolved

numerical simulations in detail. This study is performed on highly idealized prototype models where all the dynamics and approximations are transparent; these models are chosen carefully to mimic important features of potential applications in atmospheric science for the issues and approaches described above in the second and third paragraphs of this introduction. The authors hope that the results presented below will stimulate direct applications of the method to more realistic problems in atmosphere–ocean science. The contents of the remainder of the paper are outlined briefly below.

The core nonlinear dynamics of atmospheric GCMs is dominated by the quadratically nonlinear exchange of energy among modes through triad interaction. In the models in section 2, the nonlinear dynamics on the climate modes are simple prototype dynamics with either stable nonlinear periodic oscillations or multiple equilibria mimicking the scenarios discussed earlier in the third paragraph for low-frequency variability (Ghil and Robertson 2002); the exchange of energy between resolved and unresolved modes is given by a single triad interaction where the unresolved modes are stochastically forced. The stochastic mode elimination procedure (MTV-2) is applied to these models to predict the reduced stochastic climate model and then compared with the results of direct numerical simulation for several examples with predicted multiplicative and/or additive noises and augmented nonlinearity; the results reported later indicate that the nonlinear climate dynamics can be altered in a remarkable fashion through such effects. In this way, the applicability of the second step of the approximation procedure is documented. The examples from section 2 have 3 degrees of freedom. In section 3, these basic models are embedded in a fully deterministic system with over 100 degrees of freedom; in this way, the important issue of stochastic consistency, the first step of the systematic strategy (MTV-1; MTV-2) is assessed in a transparent fashion. Finally, in section 4, the a priori stochastic modeling strategy is applied for spectrally truncated quasigeostrophic flow in periodic geometry to an idealized problem analogous to the stochastic modeling of the effects of mountain torque on the angular momentum budget (Carnevale and Frederiksen 1987; Weickmann et al. 2000; Egger 2001). The systematic stochastic modeling strategy as applied in section 4 predicts a nonlinear stochastic equation for the analogue of variations in angular momentum. By comparison it is demonstrated that this equation predicts a substantially improved correlation structure for the analogue of variations in angular momentum beyond the expected linear stochastic model for a range of topographic amplitudes. A pedagogical discussion of this new application of the basic strategy (MTV-1; MTV-2) is presented in the appendix for the interested reader. The results presented here, emphasizing nonlinearity in the climate variables and testing the stochastic modeling strategy, are complementary to those results (Majda et al. 2002, hereafter MTV-3) presented recently to test the theory when nonlinear climate effects are completely absent and multiple interactions with the unresolved modes are the dominant feature.

2. Nonlinear climate dynamics for triad models

When the core dynamics of a typical atmospheric model for the midlatitudes is written in terms of an orthogonal basis (spectral or empirical such as EOF's, etc.) the principal nonlinear interactions involve the quadratically nonlinear exchange of energy. The projection of these equations on three modes yields the triad equations for $\mathbf{z} = (z_1, z_2, z_3)$, given by

$$\frac{dz_1}{dt} = b_1 z_2 z_3,$$

$$\frac{dz_2}{dt} = b_2 z_3 z_1,$$

$$\frac{dz_3}{dt} = b_3 z_2 z_1, \qquad b_1 + b_2 + b_3 = 0, \tag{2.1}$$

and the nonlinear dynamics involves a superposition of such interacting systems (Lorenz 1963; Obukhov and Dolzhansky 1975; Gluhovsky and Tong 1999; MTV-2). Here the triad models are utilized to give a simplified representation of typical nonlinear interactions occurring between resolved climate variables, denoted by **x**, and the unresolved variables **y**. The interesting and important topic of systematic procedures to determine the group of resolved climate variables and unresolved variables is not discussed (Selten 1997; Achatz and Branstator 1999) but such a form is assumed at the outset of the discussion. The focus here is the new phenomena and the quantitative validation of the stochastic mode elimination procedure when the climate variables have explicit nonlinear dynamics with either multiple equilibria or stable periodic oscillations (Ghil and Robertson 2002). Since multiplicative noises are not used commonly in regression fitting of reduced climate models at the present time, the first example studied next involves these predicted effects from the systematic mode elimination procedure.

a. Stable periodic orbit in the triad model

The standard nonlinear dynamics with a stable periodic oscillation is given by the simple system of two nonlinear equations

$$\frac{dx_1}{dt} = \lambda x_1(1 - \alpha_0|\mathbf{x}|^2) - x_2(\alpha + \beta|\mathbf{x}|^2),$$

$$\frac{dx_2}{dt} = \lambda x_2(1 - \alpha_0|\mathbf{x}|^2) + x_1(\alpha + \beta|\mathbf{x}|^2), \tag{2.2}$$

where $\mathbf{x} = (x_1, x_2)$, $|\mathbf{x}|^2 = x_1^2 + x_2^2$, and $\alpha_0 > 0$. The equations in (2.2) have a stable periodic orbit given explicitly by

$$\mathbf{x}(t) = \alpha_0^{-1/2}(\cos\omega t, \sin\omega t), \tag{2.3}$$

with frequency $\omega = \alpha + \beta\alpha_0^{-1}$. How much are the properties of such a stable periodic orbit in the reduced climate variables changed by interactions with the unresolved variables? Assume that the nonlinear interactions between two climate variables and a single unresolved variable are given by (2.1). Then the simplest triad model to address these issues is given by

$$\frac{dx_1}{dt} = b_1x_2y + \varepsilon[\lambda x_1(1 - \alpha_0|\mathbf{x}|^2) - x_2(\alpha + \beta|\mathbf{x}|^2)],$$

$$\frac{dx_2}{dt} = b_2x_2y + \varepsilon[\lambda x_2(1 - \alpha_0|\mathbf{x}|^2) + x_1(\alpha + \beta|\mathbf{x}|^2)],$$

$$\frac{dy}{dt} = b_3x_2x_1 - \frac{1}{\varepsilon}y + \sqrt{\frac{2}{\varepsilon}}\dot{W}. \tag{2.4}$$

Here and elsewhere $\dot{W}$ denotes white noise, $\langle\dot{W}\rangle = 0$, $\langle\dot{W}(t)\dot{W}(t')\rangle = \delta(t - t')$. The parameter ε in (2.4) simultaneously measures two effects: the strength of the stochastic forcing and damping of the unresolved mode and the fact that the timescale of the periodic motion in the nonlinear climate dynamics occurs on a longer timescale. Note that consistent with the summary discussion in the introduction, no stochastic terms have been introduced in the climate variables alone; in fact, the goal is to derive such stochastic effects on the coarse-grained climate timescale. The systematic mode elimination procedure (theorem 4.3 in MTV-2) rigorously predicts for $\varepsilon \ll 1$ the following reduced stochastic model for the climate variables alone on the coarse-grained climate timescale

$$\frac{dx_1}{dt} = b_1b_2x_1 + b_3b_1x_2^2x_1 + \sqrt{2}b_1x_2\dot{W} + \lambda x_1(1 - \alpha_0|\mathbf{x}|^2) - x_2(\alpha + \beta|\mathbf{x}|^2),$$

$$\frac{dx_2}{dt} = b_1b_2x_2 + b_3b_2x_1^2x_2 + \sqrt{2}b_2x_1\dot{W} + \lambda x_2(1 - \alpha_0|\mathbf{x}|^2) + x_1(\alpha + \beta|\mathbf{x}|^2). \tag{2.5}$$

Here and elsewhere in the paper, all stochastic equations are interpreted in the Itô sense (Gardiner 1985). Thus, the systematic mode elimination procedure predicts the stochastic climate model in (2.5) where the equations in (2.2) for the stable periodic orbit are modified through both augmented nonlinearity and multiplicative noise in a specific quantitative fashion. What are the new phenomena in (2.5) compared with those in (2.2) and how accurately does the reduced model in (2.5) represent the dynamics in (2.4) for fixed finite values of ε?

To address this issue, numerical simulations of (2.4) and the reduced stochastic model were developed for the following parameters in (2.4):

$$b_1 = -0.75, \quad b_2 = -0.25, \quad b_3 = 1 \quad \lambda = 0.7,$$
$$\alpha_0 = 0.8, \quad \alpha = 0.06, \quad \beta = 0.05. \tag{2.6}$$

With these parameters, the stable periodic orbit has amplitude $|\mathbf{x}| = \alpha_0^{-1/2} \simeq 1.118$. Here and elsewhere in the paper, the nonlinear terms are integrated through the second-order Runge–Kutta method, while the strong Milstein scheme of order one is utilized for the stochastic terms (Kloeden and Platen 1995). Statistics for (2.4) and (2.5) were calculated by time averaging an individual solution integrated over a long time of the order of $T = 10^5$. In this experiment as well as the others reported in this section, the parameter ε was varied systematically with values $\varepsilon = 0.125, 0.25, 0.5, 1$. In Fig. 1, a contour plot for the joint probability density function (PDF) of the climate variables x_1 and x_2 predicted by the reduced model is compared with the full system for values $\varepsilon = 0.25, 0.5, 1$. Note that the reduced model predicts two large peaks in the PDF along the x_2 axis rather than the radially symmetric PDF one might expect from the stable periodic orbit in (2.2), (2.3); also note that this predicted PDF from the reduced model agrees very well with the PDFs in the full triad model in (2.4) even for values of $\varepsilon = 1$. In Fig. 2 the time correlation functions for x_1 and x_2 for the reduced model and the full triad system are compared for $\varepsilon = 0.5$ and $\varepsilon = 1$. Once again the agreement is excellent, especially considering that (2.5) is rigorously valid only for $\varepsilon \ll 1$; the cases with $\varepsilon = 0.125$ and $\varepsilon = 0.25$ are not depicted here because the two curves are indistinguishable. A notable feature of these correlation functions is their oscillatory character; how do these oscillation frequencies in the correlation functions compare to the corresponding frequency in the stable periodic orbit in (2.2), (2.3)? The frequency of the stable periodic orbit in (2.3) is 0.1159 while the oscillation frequencies in the correlation functions for x_1 and x_2 are 0.18 and 0.14, respectively, that is, as much as 50% larger. Note that the reduced equation in (2.5) predicts asymmetry in x_1, x_2 due to the effect of nonlinear interaction with the unresolved modes. A more stringent test for the higher-order statistical behavior of the model involves the normalized correlation of energy in time for an individual mode (MTV-3),

$$K_j(t) = \frac{\langle x_j^2(t + s)x_j^2(s)\rangle}{\langle x_j^2\rangle^2 + 2\langle x_j(t + s)x_j(s)\rangle^2}, \qquad j = 1, 2. \tag{2.7}$$

The statistical quantity $K_j(t)$ is normalized so that $K_j(t) = 1$ for Gaussian variables; thus, $K_j(t)$ is an interesting test for departures from Gaussianity and the capability of the reduced stochastic model to capture such effects in a larger system. The behavior of $K_j(t)$ for the triad model for $\varepsilon = 0.5, 1$ and the reduced equations is presented in Fig. 3. Significant features in this figure are the strong departures from Gaussianity that persist over nearly a correlation time (see Fig. 2), and the capability of the reduced model to accurately track these departures even for $\varepsilon = 1$.

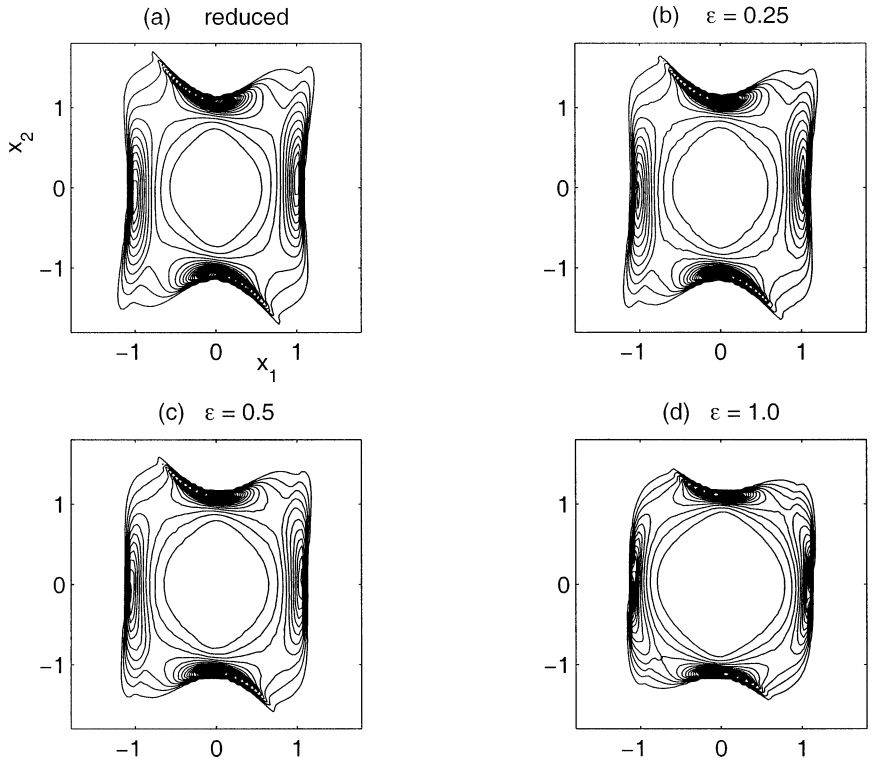

FIG. 1. Stochastic triad model with stable periodic orbit; contour plot of the joint PDF for the climate variables (x_1, x_2) for the reduced stochastic model in (2.5) and the stochastic triad equations in (2.4) with $\varepsilon = 0.25, 0.5, 1$. See Fig. 8 for the rough size of the peaks independent of ε. The large peaks are along the x_2 axis.

b. Multiple equilibria in the trial model

The simplest canonical bifurcation equation with multiple equilibria for the climate dynamics is the nonlinear equation

$$\frac{dx}{dt} = \lambda(x - \alpha x^3), \tag{2.8}$$

arising from pitchfork bifurcation. For any parameter values with $\lambda > 0$, $\alpha > 0$ the equation in (2.8) has two stable equilibria at $x = \pm\sqrt{\alpha}$ and an unstable equilibrium at $x = 0$. The parameter α controls the strength of the nonlinear contributions compared to the linear ones in the simplified climate dynamics, while λ measures the reciprocal of the overall timescale for the climate dynamics. Another prominent canonical equation for the reduced climate dynamics is the system of two equations arising from saddle node bifurcation (Ghil and Childress 1987). To assess the interaction of the climate dynamics with the unresolved modes in the simpler situation in (2.8), the following triad model is studied here:

$$\begin{aligned}
\frac{dx}{dt} &= b_1 y_2 y_3 + \varepsilon\lambda(x - \alpha x^3),\\
\frac{dy_1}{dt} &= b_2 y_2 x - \frac{1}{\varepsilon\delta} y_1 + \sqrt{\frac{2}{\varepsilon\delta}}\dot{W}_1,\\
\frac{dy_2}{dt} &= b_3 y_1 x - \frac{1}{\varepsilon} y_2 dt + \sqrt{\frac{2}{\varepsilon}}\dot{W}_2.
\end{aligned} \tag{2.9}$$

In (2.9) the parameter δ measures the fact that the two

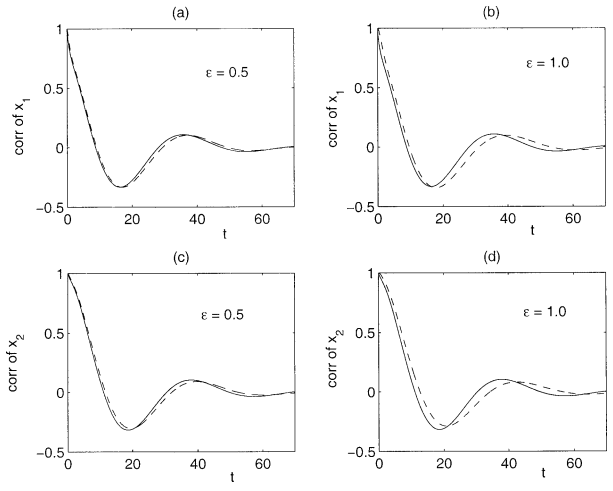

FIG. 2. Stochastic triad model with stable periodic orbit; correlation functions of x_1 and x_2 for the reduced stochastic model in (2.5) (solid lines) and the stochastic triad model in (2.4) (dashed lines) with $\varepsilon = 0.5, 1.0$.

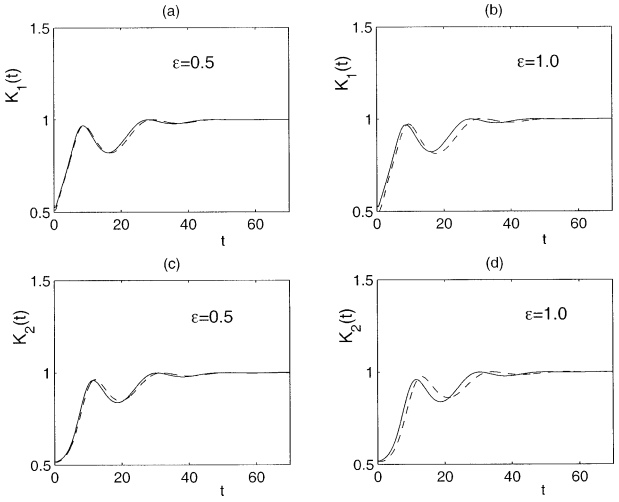

FIG. 3. Stochastic triad model with stable periodic orbit; correlation of energy $K_{1,2}(t)$ for x_1 and x_2 for the reduced stochastic model in (2.5) (solid lines) and the stochastic triad model in (2.4) (dashed lines) with $\varepsilon = 0.5, 1.0$.

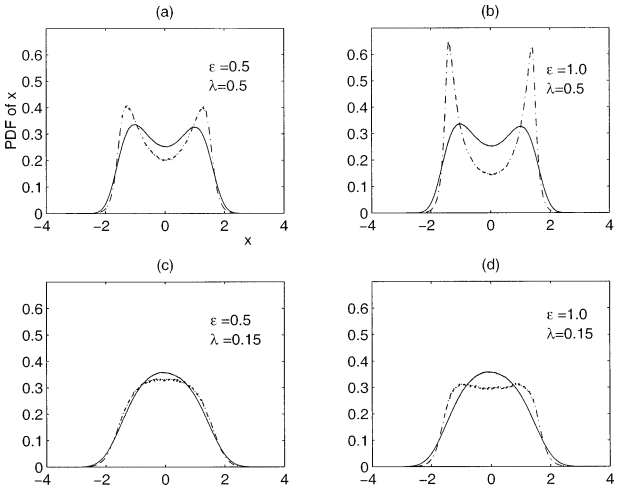

FIG. 4. Stochastic triad model with multiple equilibria; PDF for the climate variable x for the reduced equation in (2.10) (solid lines) and stochastic triad model in (2.10) (dashed lines), with $\lambda = 0.5$ (double-well regime) and $\lambda = 0.15$ (nearly Gaussian regime).

unresolved modes might be damped and forced with different strength. In this case, the systematic mode elimination strategy (theorem 4.3 in MTV-2), valid for $\varepsilon \ll 1$, predicts the following reduced stochastic equation for the climate variable x:

$$\frac{dx}{dt} = -\gamma_c x + \sigma_c \dot{W} + \lambda(x - \alpha x^3),$$

$$\gamma_c = 2\sigma_c^2 = (b_1 + b_2)^2/(1 + \delta^{-1}). \qquad (2.10)$$

Here the predicted model has additive noise. In this model, the reduced equation in (2.10) has an explicit PDF, which can be computed as a stationary solution of the associated Fokker–Planck equation (Gardiner 1985). It is given by

$$P_c = C \exp[-V(x)/2\sigma_c^2],$$

$$V(x) = \frac{1}{2}(\gamma_c - \lambda)x^2 + \frac{1}{4}\alpha\lambda x^4, \qquad (2.11)$$

where C is a normalization constant. With (2.10) and (2.11), the reduced stochastic model for the climate variable alone predicts behavior ranging from an essentially Gaussian density to a strongly peaked PDF at the two stable equilibria, and this depends in an interesting fashion on both the explicit nonlinear coupling with the unresolved modes through γ_c and σ_c and also the value of λ. To check whether these predictions are satisfied in the complete triad model, the statistics for numerical solutions of (2.9) and (2.10) were computed with the values of b_1, b_2, b_3 from (2.6), $\delta = 0.75$, $\alpha = 0.5$, and two different values of λ; $\lambda = 0.5$ with a predicted double-peaked PDF, and $\lambda = 0.15$ with a predicted nearly Gaussian PDF. As before, the parameter range $\varepsilon = 0.125, 0.25, 0.5, 1$ was utilized for the triad model in (2.9), but results are only presented below for the large values, $\varepsilon = 0.5, 1$; the discrepancies of the predictions for $\varepsilon = 0.125, 0.25$ are insignificant and the agreement between (2.9) and (2.10) is excellent. In Fig. 4 the PDF for the climate variable predicted by (2.11) is compared with the PDF for the climate variable calculated numerically from (2.9) for $\varepsilon = 0.5, 1$ and the two different values of λ. For the double-well regime, with $\lambda = 0.5$, the full triad model has sharper peaks at the stable equilibria than the prediction of the reduced model and these peaks increase with ε; nevertheless, the prediction of the reduced stochastic model is qualitatively accurate. For the case with $\lambda = 0.15$ with a predicted Gaussian PDF, the predictions of the stochastic model are accurate for $\varepsilon = 0.5$ but deteriorate somewhat for the larger value $\varepsilon = 1$. The correlation function of the climate variable x and the normalized energy correlation function $K(t)$ from (2.7) for the reduced stochastic model and the full triad model are presented in Figs. 5 and 6, respectively, for the two values $\lambda = 0.5$, $\lambda = 0.15$, and $\varepsilon = 0.5, 1$. For $\varepsilon = 0.5$ the agreement in these statistics is excellent while larger errors occur for $\varepsilon = 1$ without any strong dependence on the value of λ.

3. Stochastic consistency with nonlinear climate dynamics and many degrees of freedom

As summarized in the introduction, the systematic mode reduction strategy (MTV-1; MTV-2) has two steps: stochastic consistency and stochastic-mode elimination. In section 2 various facets and predictions of the second step involving mode elimination have been tested for prototype models with nonlinear climate dynamics and 3 degrees of freedom. Here the same predictions and issues are studied for model deterministic systems with over 100 degrees of freedom but with the same projected nonlinear climate dynamics as the two

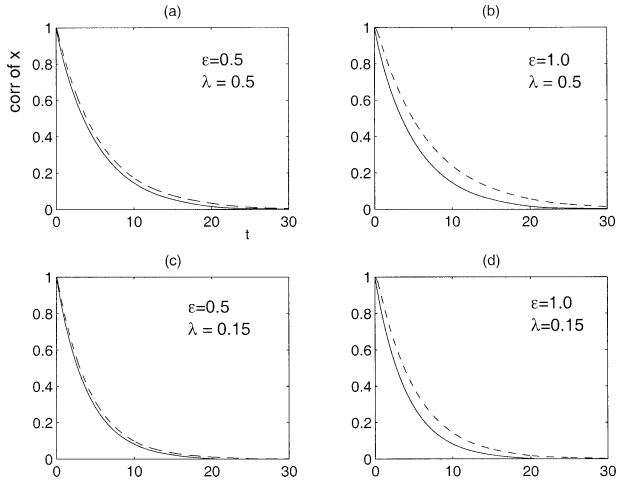

FIG. 5. Stochastic triad model with multiple equilibria; correlation function of x for the reduced equation in (2.10) (solid lines) stochastic triad model in (2.10) (dashed lines), with $\lambda = 0.5$ (double-well regime) and $\lambda = 0.15$ (nearly Gaussian regime).

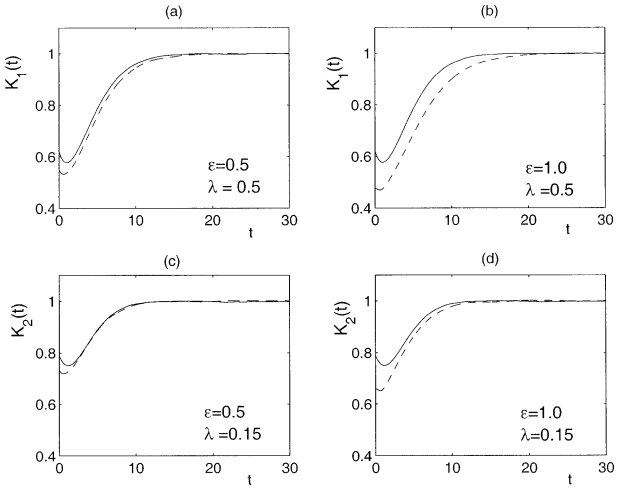

FIG. 6. Stochastic triad model with multiple equilibria; non-Gaussianity test $K(t)$ for x for the reduced equation in (2.10) (solid lines) and the stochastic triad model in (2.10) (dashed lines), with with $\lambda = 0.5$ (double-well regime) and $\lambda = 0.15$ (nearly Gaussian regime); $K \equiv 1$ corresponds to Gaussian behavior.

models in section 2. Thus, the results in section 2 provide a simplified context for the material presented here. The main new issue addressed here is an unambiguous test of stochastic consistency, which involves approximation of the self-interaction terms among the unresolved variables by white noise stochastic forcing and damping; in chaotic dynamical systems with many degrees of freedom and sensitive dependence on small perturbations in the unresolved modes, this is anticipated to be a reasonable approximation provided that coarse-grained modeling on longer timescales, as for climate, is the goal.

The deterministic prototype ''toy'' models introduced here for these purposes are built in a simple fashion. The main idea is to use the same low-order triad models in (2.4) and (2.9) but to replace the strong damping and white noise forcing for the unresolved variables, y in (2.4) and y_1, y_2 in (2.9), by deterministic quadratic nonlinear interactions coupling these modes to many other deterministic degrees of freedom. Here, the Galerkin projection of the inviscid Burgers equation, $u_t + uu_x = 0$, is utilized for these purposes; these equations are a strongly chaotic system with many degrees of freedom, an interesting range of equipartition of energy spectrum, and correlation scaling laws that are predicted successfully by simple scaling theories (Majda and Timofeyev 2000). If the complex Fourier amplitudes $\hat{u}_k = y_k + iz_k$ are introduced for $1 \le |k| \le \Lambda$ with $\hat{u}_{-k} = \hat{u}_k^*$,these equations are given by

$$\frac{dy_k}{dt} = -\mathrm{Re}\frac{ik}{2}\sum_{p+q+k=0}\hat{u}_p^*\hat{u}_q^*,$$

$$\frac{dz_k}{dt} = -\mathrm{Im}\frac{ik}{2}\sum_{p+q+k=0}\hat{u}_p^*\hat{u}_q^*. \qquad (3.1)$$

The equations in (3.1) with $\Lambda = 50$ are integrated efficiently later through a standard pseudospectral method in space and fourth-order Runge–Kutta method in time (Majda and Timofeyev 2000).

a. Stable periodic orbits with many degrees of freedom

With the motivation from the previous paragraph, the deterministic model considered here with 102 degrees of freedom ($1 \le k \le \Lambda$) is given by

$$\frac{dx_1}{dt} = \overline{\lambda}b_1x_2y_1 + \lambda x_1(1 - \alpha_0|\mathbf{x}|^2) - x_2(\sigma + \beta|\mathbf{x}|^2),$$

$$\frac{dx_2}{dt} = \overline{\lambda}b_2x_1y_1 + \lambda x_2(1 - \alpha_0|\mathbf{x}|^2) + x_1(\alpha + \beta|\mathbf{x}|^2),$$

$$\frac{dy_k}{dt} = -\mathrm{Re}\frac{ik}{2}\sum_{p+q+k=0}\hat{u}_p^*\hat{u}_q^* + \overline{\lambda}b_3\delta_{1,k}x_1x_2,$$

$$\frac{dz_k}{dt} = -\mathrm{Im}\frac{ik}{2}\sum_{p+q+k=0}\hat{u}_p^*\hat{u}_q^*, \qquad (3.2)$$

where $|\mathbf{x}|^2 = x_1^2 + x_2^2$ and $\delta_{1,k} = 1$ for $k = 1$ and 0 otherwise. The deterministic equations in (3.2) projected on the three variables (x_1, x_2, y_1) essentially coincide with the nonlinear dynamics in (2.4) without stochastic forcing and damping. In the first step of the stochastic modeling strategy, the deterministic nonlinear interaction terms for y_1 are approximated as follows:

$$-\mathrm{Re}\frac{i}{2}\sum_{p+q+1=0}\hat{u}_p^*\hat{u}_q^* \approx -\gamma_1y_1 + \sigma_1\dot{W},$$

$$\frac{\sigma_1^2}{2\gamma_1} = \mathrm{var}\{y_1\}. \qquad (3.3)$$

TABLE 1. Many degrees of freedom system with stable periodic orbit; low-order statistics for the climate varibles x_1 and x_2; CT denoted correlation time.

	DNS	Reduced
Mean$\{x_1\}$	0.006	−0.0003
Var$\{x_1\}$	0.38	0.35
Flatness$\{x_1\}$	2.15	2.31
CT$\{x_1\}$	10.96	10.52
Mean$\{x_2\}$	−0.004	−0.004
Var$\{x_2\}$	0.79	0.82
Flatness$\{x_2\}$	1.27	1.23
CT$\{x_2\}$	20.16	24.42

With the approximation in (3.3) the equations in (3.2) become essentially the stochastic model in (2.4) with minor changes; applying the stochastic mode elimination procedure [theorem (4.3) of MTV-2] yields the reduced stochastic model for the climate variables x_1, x_2 given by

$$\frac{dx_1}{dt} = N_1 x_1 x_2^2 + \overline{\sigma}_1 x_2 \dot{W} + \lambda x_1(1 - \alpha_0|\mathbf{x}|^2) - x_2(\alpha + \beta|\mathbf{x}|^2),$$

$$\frac{dx_2}{dt} = N_2 x_2 x_1^2 + \overline{\sigma}_2 x_1 \dot{W} + \lambda x_2(1 - \alpha_0|\mathbf{x}|^2) + x_1(\alpha + \beta|\mathbf{x}|^2), \tag{3.4}$$

where

$$N_1 = \overline{\lambda}^2 b_1 b_3 \gamma_1^{-1}, \qquad N_2 = \overline{\lambda}^2 b_2 b_3 \gamma_1^{-1},$$

$$\overline{\sigma}_1 = \overline{\lambda} b_1 \frac{\sigma_1}{\gamma_1}, \qquad \overline{\sigma}_2 = \overline{\lambda} b_2 \frac{\sigma_1}{\gamma_1}.$$

This reduced model has the same features as the one in (2.5) but arises now as the reduced two-dimensional model in a system with 102 degrees of freedom. For the same values in (2.6) for the coefficients and $\overline{\lambda} = 2$ the deterministic equations in (3.2) are integrated for times of the order of $T = 10^5$ and statistics are computed from this solution. In this damped driven system, the modes y_k, z_k, $1 \le k \le \Lambda$ all achieve equipartition of energy with a variance 0.2525 within 1%. The coefficient γ_1 is determined crudely as the inverse of the area under the graph of the modulus of the correlation function for y_1, while σ_1 is determined through γ_1 and the variance of y_1 through the equation $\sigma_1^2(2\gamma_1) = \text{var}\{y_1\}$; the values are $\gamma_1 = 2.7671$, $\sigma_1 = 1.1803$. These formulas completely determine the reduced stochastic model in (3.4). Table 1 compares the low-order statistics of the climate variables x_1, x_2 calculated from the direct numerical simulation (DNS) of (3.2) and the numerical integration of the reduced stochastic model in (3.4); in Table 1 the correlation times are computed as the reciprocal of the integral of the modulus of the correlation function. Note that the flatness is the ratio of the fourth moment to the second moment squared. All of the low-order statistics of x_1 and x_2 are computed accurately by the reduced stochastic model; the largest errors are about 20% in the correlation time for x_2 with significantly smaller errors for all the other quantities. The joint PDF of the variables x_1, x_2 for both the DNS and the reduced stochastic model are shown in Fig. 7 while the marginal PDFs for x_1 and x_2 are compared in Fig. 8; clearly both the structure of the PDF and the quantitative amplitude of the peaks are captured remarkably well by the reduced stochastic model. Note from Fig. 8 that the PDF peaks along the x_2 axis are very large while those along the x_1 axis are insignificant. Figure 9 compares the correlation matrix of x_1, x_2 and the normalized correlation function of the energy in x_2, $K_2(t)$ from (2.7). All the approximations are excellent given the a priori nature of the reduced model, including the highly non-Gaussian long-tail behavior exhibited by $K_2(t)$; $K_1(t)$ exhibits more rapid adjustment to the Gaussian level, $K_1(t) \equiv 1$, and is not displayed here. Finally note from Figs. 9a

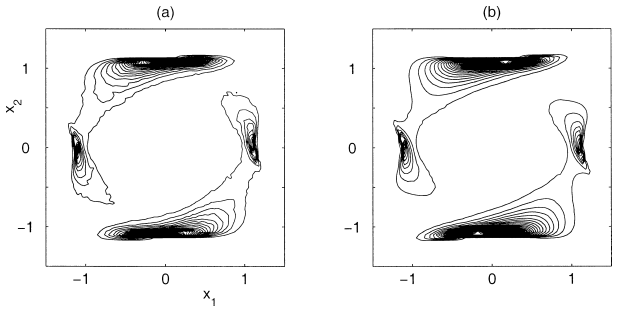

FIG. 7. Stable periodic orbit with many degrees of freedom; contour plots of the joint probability density for the climate variables x_1 and x_2; (a) deterministic system with 102 variables in (3.2); (b) reduced stochastic equation in (3.4). See Fig. 8 for the size of the fourth peaks. The large peaks are along the x_2 axis.

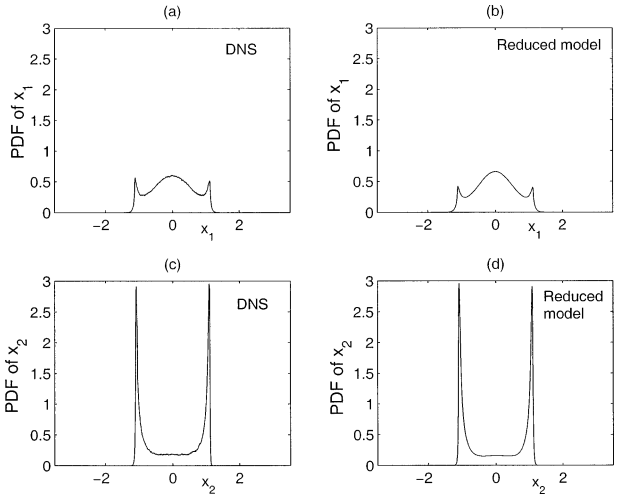

FIG. 8. Stable periodic orbit with many degrees of freedom; marginal PDFs of x_1 and x_2 for the simulations of the full equations in (3.2) and reduced stochastic model in (3.4). (a), (c) DNS stands for direct numerical simulations.

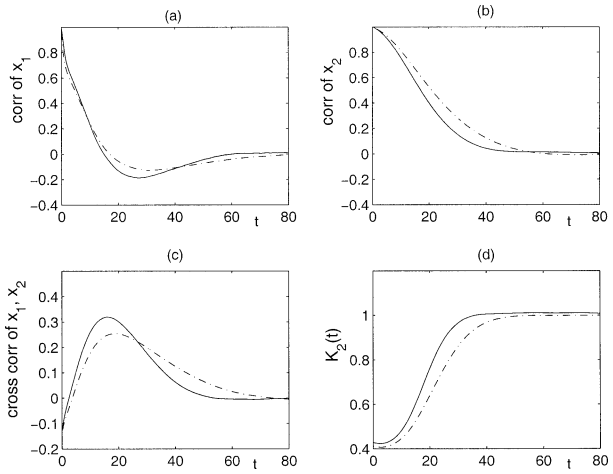

FIG. 9. Stable periodic orbit with many degrees of freedom; two-point statistics for x_1 and x_2; deterministic system with 102 degrees of freedom (solid lines); stochastic reduced equation (dashed lines); (a),(b) correlation function of x_1 and x_2, respectively; (c) cross-correlation function of x_1 and x_2; (d) normalized correlation of energy $K_2(t)$ in x_2.

and 9b that neither correlation function for x_2 has a significant oscillatory component representing the ghost of the stable periodic orbit in the projected climate dynamics, but the oscillatory component of the correlation function for x_1 from the DNS has a frequency $\omega = 0.1047$, which agrees within about 10% with the frequency of the deterministic periodic orbit, $\omega = 0.1159$.

b. Multiple equilibria with many degrees of freedom

For the models with multiple equilibria, the prototype deterministic models with 101 variables are given by

$$\frac{dx}{dt} = \overline{\lambda} b_1 y_1 z_1 + \lambda(1 - \alpha x^2)x,$$

$$\frac{dy_k}{dt} = -\mathrm{Re}\frac{ik}{2}\sum_{p+q+k=0} \hat{u}_p^* \hat{u}_q^* + \overline{\lambda} b_2 \delta_{1,k} x z_k,$$

$$\frac{dz_k}{dt} = -\mathrm{Im}\frac{ik}{2}\sum_{p+q+k=0} \hat{u}_p^* \hat{u}_q^* + \overline{\lambda} b_3 \delta_{1,k} x y_k. \quad (3.5)$$

The projection on the variables (x, y_1, z_1) gives essentially the same nonlinear dynamics as for the model in (2.9) without forcing and damping provided the unresolved variables y_1, z_1 are identified with y_1, y_2 in (2.9). As in (3.3) stochastic consistency involves the approximation

$$-\mathrm{Re}\frac{i}{2}\sum_{p+q+1=0} \hat{u}_p^* \hat{u}_q^* \approx -\gamma_1 y_1 + \sigma_1 \dot{W}_1,$$

$$-\mathrm{Im}\frac{i}{2}\sum_{p+q+1=0} \hat{u}_p^* \hat{u}_q^* \approx -\gamma_1 z_1 + \sigma_1 \dot{W}_2 \quad (3.6)$$

with $\sigma_1^2/(2\gamma_1) = \mathrm{var}\{y_1\} = \mathrm{var}\{z_1\}$. With the approximations in (3.6), the equations in (3.5) become essentially the stochastic model in (2.9) with minor changes and the stochastic mode elimination procedure yields the following reduced stochastic model for the climate variables

$$\frac{dx}{dt} = -\gamma_c x + \sigma_x \dot{W} + \lambda(1 - \alpha x^2)x, \quad (3.7)$$

where

$$\gamma_c = \frac{\overline{\lambda}^2 b_1^2 \sigma_1^2}{4\gamma_1^2}, \qquad \sigma_c^2 = \sigma_1^2 \frac{\gamma_c}{\gamma_1}.$$

Recall from section 2 that the parameter λ determines the structure of the PDF of x as in (2.11); the three values $\lambda = 0.15, 0.5, 1.2$ are considered in the numerical simulations of the deterministic model in (3.5) with $\overline{\lambda} = 3$ and the same remaining parameters from section 2b. The 96 modes y_k, z_k with $k \geq 3$ exhibit equipartition of energy within 2% for three different values of λ. Table 2 lists the quantities $\mathrm{var}\{y_1\}$ and correlation time of y_1 for the three cases that are utilized for computing the values of γ_c, σ_c needed for the reduced stochastic model in (3.7). The value of ε in Table 2 was determined by comparing (3.7) with (2.9) utilizing the largest interaction coefficient, $b_3 = 1$, to yield $\varepsilon \approx \overline{\lambda}\,\mathrm{var}\{x\}\gamma_1^{-1} \approx 0.5$. The low-order statistics for climate variable x in the DNS and predicted by the reduced stochastic model are in excellent agreement for all three cases. The PDFs for the deterministic system and the one-dimensional reduced stochastic model for the three cases are presented in Fig. 10. As anticipated by the results in section 2b for $\varepsilon \approx 0.5$, the one-dimensional stochastic model captures the transition behavior in the PDF of the deterministic system from peaks at the stable equilibria to a nearly Gaussian PDF as λ decreases. As can be anticipated from Table 2, both the correlation

TABLE 2. Many degrees of freedom system with multiple equilibria; low-order statistics for the climate variable x and the first unresolved mode Y_1.

	Mean$\{x\}$	Var$\{x\}$	Flat$\{x\}$	Var$\{y_1\}$	CT$\{x\}$	CT$\{y_1\}$	ε
DNS $\lambda = 1.2$	−0.0037	1.21	1.55	1.04	3.65	0.17	0.56
Reduced $\lambda = 1.2$	0.01	1.12	1.75	N/A	3.38	N/A	
DNS $\lambda = 0.5$	0.012	0.974	1.892	0.852	3.36	0.18	0.55
Reduced $\lambda = 0.5$	0.01	0.91	2.09	N/A	3.22	N/A	
DNS $\lambda = 0.15$	0.0001	0.72	2.39	0.67	3.58	0.21	0.53
Reduced $\lambda = 0.15$	0.01	0.70	2.53	N/A	3.32	N/A	

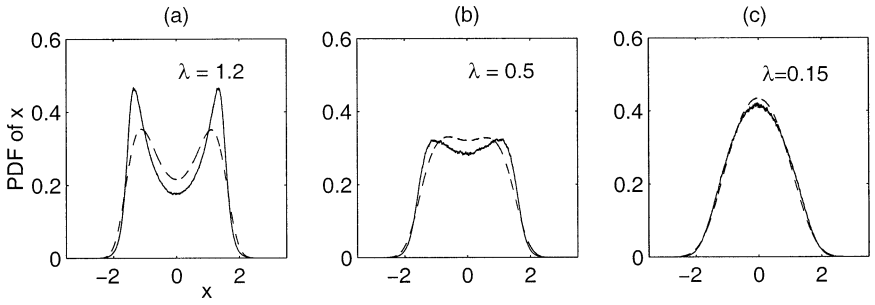

FIG. 10. Multiple equilibria with many degrees of freedom; PDF for the climate variable x for the simulations of the deterministic model in (3.5) (solid lines) and the reduced equation in (3.7) (dashed lines) in three regimes, $\lambda = 1.2, 0.5, 0.15$; (c) the solid and dashed lines nearly overlap in the regime $\lambda = 0.15$.

function for the climate mode and the normalized correlation function for the energy in the climate mode $K(t)$, depicted in Fig. 11 for the three cases, have only small discrepancies between the DNS and the single-variable reduced stochastic model. Note by comparing Fig. 9d and Fig. 11 for the three cases that the departures from Gaussianity measured by $K(t)$ are much stronger for both the reduced model and DNS for multiplicative noise in the reduced model as compared with the three additive noise cases presented here.

4. A priori stochastic modeling for topographic stress

The ideal barotropic quasigeostrophic equations with a large-scale zonal mean flow U on a $2\pi \times 2\pi$ periodic domain (Carnevale and Frederiksen 1987) are given by

$$\frac{\partial q}{\partial t} + \nabla^{\perp}\psi \cdot \nabla q + U\frac{\partial q}{\partial x} + \beta\frac{\partial \psi}{\partial x} = 0,$$
$$q = \Delta\psi + h,$$
$$\frac{dU}{dt} = \frac{1}{4\pi^2}\int h\frac{\partial \psi}{\partial x}\,dx\,dy, \tag{4.1}$$

where q is the potential vorticity, U is the large-scale zonal mean flow, ψ is the streamfunction, and h is the topography. In (4.1), the mean flow changes in time through the topographic stress; this effect is the direct analogue for periodic geometry of the change in time of angular momentum due to mountain torque in spherical geometry (Frederiksen et al. 1996). Here the a priori stochastic modeling strategy (MTV-1; MTV-2) is applied to the stochastic modeling of the topographic stress terms in (4.1) as an analogue for mountain torque; thus, the variable U is the resolved variable while all the modes ψ_k are unresolved variables for the general stochastic modeling strategy as summarized in the introduction and applied earlier in sections 2 and 3. Given that U responds linearly to the streamfunction in (4.1), naively, one might anticipate that the predicted stochastic model for U is a linear Langevin equation with damping and white noise forcing. Surprisingly, the new application of the stochastic modeling strategy developed later yields a nonlinear stochastic equation for U; furthermore, numerical simulations reveal an improved prediction of the correlation function for U beyond a purely linear stochastic model. The equations in (4.1) are expanded in Fourier modes with $f_{\mathbf{k}}$ denoting the $\mathbf{k}$th Fourier coefficient of a 2π-periodic function f with $\mathbf{k} = (k_x, k_y)$ and truncated to $|\mathbf{k}|^2 \le \Lambda$. The truncated equations conserve the two quadratic invariants, energy and enstrophy, and have a family of Gaussian invariant measures (Carnevale and Frederiksen 1987), depending on two parameters, α, $\mu > 0$ with

$$\overline{U} = \text{mean}\{U\} = -\frac{\beta}{\mu},$$
$$\text{var}\{U\} = \frac{1}{\alpha\mu},$$
$$\overline{\psi}_{\mathbf{k}} = \text{mean}\{\psi_{\mathbf{k}}\} = -\frac{h_{\mathbf{k}}}{\mu + |\mathbf{k}|^2},$$
$$\text{var}\{\psi_{\mathbf{k}}\} = \frac{1}{\alpha|\mathbf{k}|^2(\mu + |\mathbf{k}|^2)}. \tag{4.2}$$

The predicted mean state in (4.2) is nonlinearly stable (Carnevale and Frederiksen 1987) and does not have topographic instability.

a. A priori stochastic model

The fully a priori strategy assumes that the climate PDF is given by the Gaussian measure defined by (4.2) for fixed α, $\mu > 0$; nondimensional variables for perturbations about the climate mean are given by

$$U^{\text{new}} = (U - \overline{U})/\sqrt{\text{var}\{U\}},$$
$$\psi_{\mathbf{k}}^{\text{new}} = (\psi_{\mathbf{k}} - \tilde{\psi}_{\mathbf{k}}/\sqrt{\text{var}\{\psi_{\mathbf{k}}\}}. \tag{4.3}$$

In the new variables, the truncated equations from (4.1) for each Fourier mode and U are given by

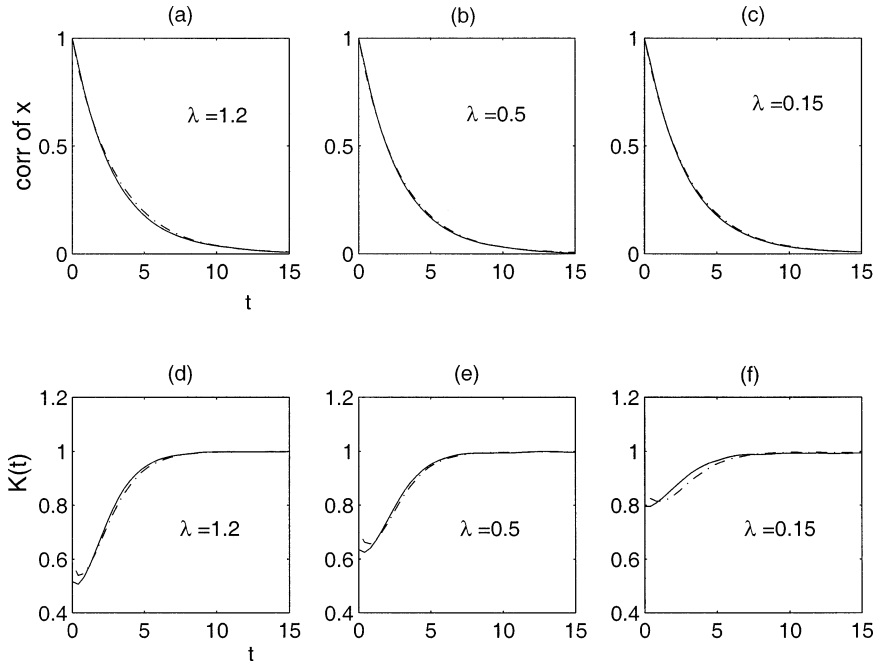

FIG. 11. Multiple equilibria with many degrees of freedom; two-point statistics of the climate variable, x, in three regimes, $\lambda = 1.2, 0.5, 0.15$ for the deterministic equations in (3.5) (solid lines) and for the reduced equation in (3.7) (dashed lines). (a),(b),(c) correlation function of x; (d),(e),(f) correlation of energy $K(t)$ in x.

$$\frac{d\psi_{\mathbf{k}}}{dt} = -i\frac{k_x}{\sqrt{\alpha\mu}}U\psi_{\mathbf{k}} + ik_xH'_{\mathbf{k}}U - i\Omega'_{\mathbf{k}}\psi_{\mathbf{k}} + \sum_{\mathbf{l},\mathbf{m}} B_{klm}\psi_{\mathbf{l}}^*\psi_{\mathbf{m}}^* + \sum_{\mathbf{l}} L_{kl}\psi_{\mathbf{l}},$$

$$\frac{dU}{dt} = 2\,\mathrm{Im}\sum_{\mathbf{k}} k_xH'_{\mathbf{k}}\psi_{\mathbf{k}}, \tag{4.4}$$

where

$$H'_{\mathbf{k}} = h_{\mathbf{k}}\sqrt{\frac{\mu}{|\mathbf{k}|^2(\mu + |\mathbf{k}|^2}},$$

$$\Omega'_{\mathbf{k}} = \frac{k_x\beta}{|\mathbf{k}|^2} - \overline{U}k_x. \tag{4.5}$$

Note that $\Omega'_{\mathbf{k}}$ is the Rossby wave frequency Doppler shifted by the mean flow. In the present application, all the $\psi_{\mathbf{k}}$ are unresolved variables; thus, the first step is to invoke the approximation of stochastic consistency,

$$\sum_{\mathbf{l},\mathbf{m}} B_{klm}\psi_{\mathbf{l}}^*\psi_{\mathbf{m}}^* + \sum_{\mathbf{l}} L_{kl}\psi_{\mathbf{l}} \approx -\gamma_{\mathbf{k}}\psi_{\mathbf{k}} + \sigma_{\mathbf{k}}\dot{W}_{\mathbf{k}}, \tag{4.6}$$

where $\sigma_{\mathbf{k}}^2/\gamma_{\mathbf{k}} = 1$, which is consistent with $\mathrm{var}\{\psi_{\mathbf{k}}\} = 1$ in the nondimensional variables. Utilizing the heuristic approximation from (4.6) in (4.4) defines the approximate stochastic model as developed earlier in section 3. In the second step of the procedure, a stochastic model elimination procedure is applied to get a stochastic equation for the climate variable U on a coarse-grained timescale. The novel feature of this modeling step in the present application rests on the observation that the contribution from the nonlinear interaction term, $ik_x(\alpha\mu)^{-1/2}U\psi_{\mathbf{k}}$, in (4.4), is often large. This is demonstrated a posteriori in the numerical tests developed later (see Figs. 13 and 14). Utilizing this fact in the systematic stochastic modeling procedure results in the predicted nonlinear reduced equation for U,

$$\frac{dU}{dt} = -\gamma(U)U + \gamma'(U) + \sqrt{2\gamma(U)}\dot{W}, \tag{4.7}$$

where $\gamma'(U) = d\gamma/dU$ and

$$\gamma(U) = 2\sum_{\mathbf{k}} \frac{k_x^2|H'_{\mathbf{k}}|^2\gamma_{\mathbf{k}}}{\gamma_{\mathbf{k}}^2 + [\Omega'_{\mathbf{k}} + k_x(\alpha\mu)^{1/2}U]^2}. \tag{4.8}$$

The details of the derivation of (4.7) are sketched in the appendix. Note that the Doppler-shifted topographic Rossby wave frequencies, Ω_k from (4.5), enter into the nonlinear corrections in the denominator in (4.8). Under the additional assumption that $(\alpha\mu)^{-1}|k_xU|^2 \ll \gamma_{\mathbf{k}}^2 + (\Omega'_{\mathbf{k}})^2$, a standard predicted linear stochastic model for U emerges from (4.7) with $\gamma = \gamma(0)$ from (4.8) and $\gamma'(0) = 0$ (MTV-1; MTV-2). Next, the performances of both the nonlinear stochastic model in (4.7) and the linear model are compared with numerical simulations.

b. Comparison with numerical simulations

In the numerical experiments reported later, the truncation $|\mathbf{k}|^2 \le \Lambda$ with $\Lambda = 17$ was utilized with 57

TABLE 3. One-point statistics for U and the real part of the first few modes $\psi_{\mathbf{k}}$ for the simulations with $H = 0.3535$ ($\max|h| = 0.5$).

	U	$\psi_{(1,0)}$	$\psi_{(0,1)}$	$\psi_{(1,1)}$	$\psi_{(1,-1)}$	$\psi_{(2,0)}$	$\psi_{(0,2)}$
DNS mean	−0.458	0.06287	0.00093	0.00024	0.00015	0.00008	0.00011
DNS variance	0.3789	0.1718	0.1737	0.0675	0.0666	0.0219	0.0221
DNS skewness	0.693	−0.0912	−0.0025	0.0093	−0.0061	0.0025	0.0008
DNS flatness	2.95	2.54	2.53	2.73	2.73	2.88	2.89
Stat mech mean	−0.5	0.05891	0	0	0	0	0
Stat mech variance	0.5	0.1666	0.1666	0.0625	0.0625	0.0208	0.0208
Reduced mean	0.5005						
Reduced variance	0.4984						
Reduced skewness	0.0258						
Reduced flatness	2.935						

degrees of freedom. Since the main contributions for fluctuations in angular momentum due to mountain torque are due to large-scale Rossby waves (Egger 2001), here $\beta = 1$ and single-mode large-scale topography,

$$h(x, y) = H[\cos(x) + \sin(x)], \tag{4.9}$$

is utilized with three amplitudes for $H = 0.3535, 0.7071, 1.06$, so that $\max|h| = 0.5, 1, 1.5$, in order to exhibit a range of behavior for the correlation functions. The use of a single topographic Rossby mode here in the model is to provide a difficult extreme test for stochastic mode reduction rather than complete fidelity to realistic topography. The truncated equations for the variables U and the single topographic mode alone have completely integrable nonlinear oscillations (Grote et al. 1998) and no stochastic behavior. Nevertheless, all of the transfer of fluctuations from the other unresolved modes to the mean flow occurs through this single Rossby mode. In the numerical simulations, the Fourier modes of the initial data had random phases and amplitudes consistent with the ensemble mean energy and enstrophy for the Gaussian measure specified by (4.2) with the prescribed μ and α; after skipping an initial time interval of the order of 2×10^4, statistics were computed from the values of this numerical solution for times of order $T = 1.5 \times 10^4$. The benchmark values $\alpha = 1$, $\mu = 2$ are utilized in all the simulations. Note that the numerical simulations are not automatically centered at the climate mean state predicted in (4.2) as a stringent test.

The theoretical equilibrium statistical predictions summarized in (4.2) are a Gaussian PDF for U and all Fourier amplitudes, $\psi_{\mathbf{k}}$; furthermore, the nonlinear stochastic model in (4.7) also has Gaussian PDF by design (MTV-2; MTV-3). See the appendix. In Tables 3, 4, and 5, the low-order single time statistics for U and Re $\psi_{\mathbf{k}}$, $|\mathbf{k}|^2 \leq 4$ from the numerical simulations are compared with the theoretical predictions from (4.2) and for the reduced stochastic model in (4.7) for $H = 0.3535$, 0.7071, 1.06. Several trends are evident: for all of the modes except U and $\psi_{(1,0)}$ the predictions of equilibrium statistical mechanics (stat mech) are excellent; the discrepancies for U are largest of order 15% in the mean and 20%–25% in the variance with somewhat smaller discrepancies for the mean and variance for $\psi_{(1,0)}$. One unexpected feature is the evident positive skewness in the PDF for U, which persists for all three cases with a weaker negative skewness in the PDF for Re $\psi_{(1,0)}$. Since the stochastic model is based on the a priori climate in (4.2), it necessarily has a Gaussian PDF and cannot account for these features.

The correlation functions for U and the modes Re $\psi_{(1,0)}$, Re $\psi_{(0,1)}$ are presented in Fig. 12 for the three topographic amplitudes. Note that the correlation time of U decreases while the correlation time of Re $\psi_{(1,0)}$ increases as the amplitude of the topography increases and these two times are comparable for the last case with $H = 1.06$ ($\max|h| = 1.5$); also, the correlation function for U tends to develop oscillations in phase with those in Re $\psi_{(1,0)}$ as the topographic amplitude increases. Recall that $\psi_{(1,0)}$ is the amplitude of the large-

TABLE 4. The same as in Table 3 except simulations with $H = 0.7071$ ($\max|h| = 1$).

	U	$\psi_{(1,0)}$	$\psi_{(0,1)}$	$\psi_{(1,1)}$	$\psi_{(1,-1)}$	$\psi_{(2,0)}$	$\psi_{(0,2)}$
DNS mean	−0.442	0.12234	−0.0044	−0.00029	0.0011	0.00055	−0.00008
DNS variance	0.382	0.16965	0.17569	0.0672	0.0675	0.0221	0.0221
DNS skewness	0.6601	−0.1818	−0.0018	−0.006	0.008	0.01	−0.009
DNS flatness	2.95	2.6	2.55	2.75	2.73	2.88	2.88
Stat mech mean	−0.5	0.11785	0	0	0	0	0
Stat mech variance	0.5	0.1666	0.1666	0.0625	0.0625	0.0208	0.0208
Reduced mean	−0.501						
Reduced variance	0.4951						
Reduced skewness	0.0114						
Reduced flatness	3.0032						

TABLE 5. The same as in Table 3 except simulations with $H = 1.06$ ($\max|h| = 1.5$).

	U	$\psi_{(1,0)}$	$\psi_{(0,1)}$	$\psi_{(1,1)}$	$\psi_{(1,-1)}$	$\psi_{(2,0)}$	$\psi_{(0,2)}$
DNS mean	−0.4455	0.18451	−0.0008	0.00019	−0.0002	0.0007	0.00008
DNS variance	0.3847	0.16706	0.1755	0.0677	0.0674	0.0221	0.0219
DNS skewness	0.682	−0.2636	0.0034	0.0017	−0.0025	0.0159	0.0074
DNS flatness	3.04	2.68	2.55	2.73	2.74	2.88	2.88
Stat mech mean	−0.5	0.17677	0	0	0	0	0
Stat mech variance	0.5	0.1666	0.1666	0.0625	0.0625	0.0208	0.0208
Reduced mean	−0.501						
Reduced variance	0.4962						
Reduced skewness	0.008						
Reduced flatness	3.01						

scale Rossby wave that interacts with the topography while $\psi_{(0,1)}$ is associated with zonal flow amplitudes so oscillatory correlations in $\psi_{(1,0)}$ and decaying correlations in $\psi_{(0,1)}$ are expected. Clearly, no simple linear Langevin stochastic model can capture the behavior of the correlations in U depicted in Fig. 12.

The nonlinear stochastic model in (4.7) and the corresponding linear model require estimated values for $\sigma_{\mathbf{k}}$ and $\gamma_{\mathbf{k}}$. The decay time $\gamma_{(1,0)}$ in (4.6) was chosen as the best fit to the correlation function of Re $\psi_{(1,0)}$ by $\exp^{-\gamma_{(1,0)}t}\cos(\Omega'_{(1,0)}t)$ with $\Omega'_{(1,0)}$ from (4.5) and $\sigma_{\mathbf{k}}$ determined from (4.2) and $\sigma_{\mathbf{k}}^2/\gamma_{\mathbf{k}} = \mathrm{var}\{\psi_{\mathbf{k}}\}$. The correlation functions for U determined by the nonlinear stochastic equation in (4.7) with these parameters and the corresponding linear stochastic model are compared with the numerical correlation functions for the three cases in Figs. 13 and 14; Fig. 14 has a logarithmic vertical scale. As is evident from these figures, the predictions of the nonlinear stochastic model are quite good with similar accuracy for all three topographic heights, including the difficult case, $\max|h| = 1.5$, where the ratio of correlation times for Re $\psi_{(1,0)}$ and U is approximately one. Furthermore, the nonlinear stochastic model has predictions that are always clearly superior to the linear stochastic model although both models have comparable asymptotic behavior for very large lag times.

5. Summary and conclusions

A systematic modeling strategy for stochastic mode reduction (MTV-1; MTV-2) has been applied here to three prototype ''toy'' models with nonlinear behavior mimicking several important features for low-frequency variability of the atmosphere. In particular, models with either stable periodic orbits or multiple equilibria in the projected climate dynamics were emphasized in sections 2 and 3. The systematic strategy has two steps: stochastic consistency and stochastic mode elimination. Both aspects of the strategy are tested in the paper in an a priori fashion; in particular, it has been established in all examples studied here that the stochastic mode elimination step, which is justified rigorously only for $\varepsilon \ll 1$, in fact applies for values of ε as large as $\varepsilon \approx 0.5$ and even $\varepsilon \approx 1$ in many situations. Since ε measures roughly the square root of the ratio of correlation times of unresolved variables to the resolved ones, these results suggest potential application of the method for reduced stochastic modeling of low-frequency variability in the atmosphere where $\varepsilon \approx 0.4$ or 0.5 (the ratio of 3 to 4 days for synoptic-scale correlations to 8 to 10 days for low-frequency variables). The results developed here provide some new perspectives on both the role of stable nonlinear structures in projected nonlinear climate dynamics and also regression fitting strategies for stochastic climate modeling.

The example in section 3a dramatically illustrates several of these points. This deterministic system with 102 degrees of freedom has an explicit periodic orbit, which is stable as regards the projected climate dynamics for the two climate variables; however, the ''ghost'' of this periodic oscillation in the complete deterministic

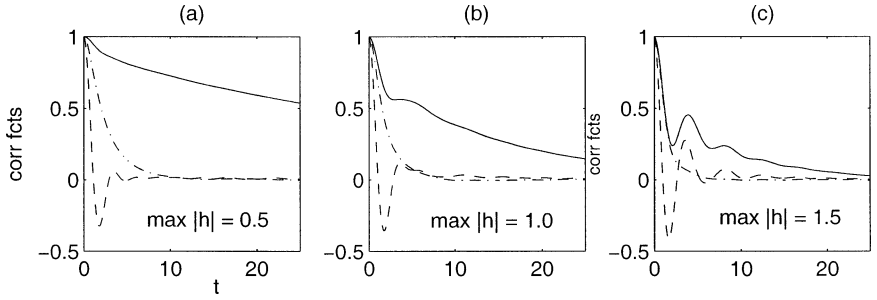

FIG. 12. Barotropic QG equation; comparison of correlation function of the mean U (solid line), Re $\psi_{1,0}$ (dashed line), and Re $\psi_{1,0}$ (dot–dashed line) for simulations of the barotropic QG equation in (4.1) for three values of $\max|h| = 0.5, 1.0, 1.5$.

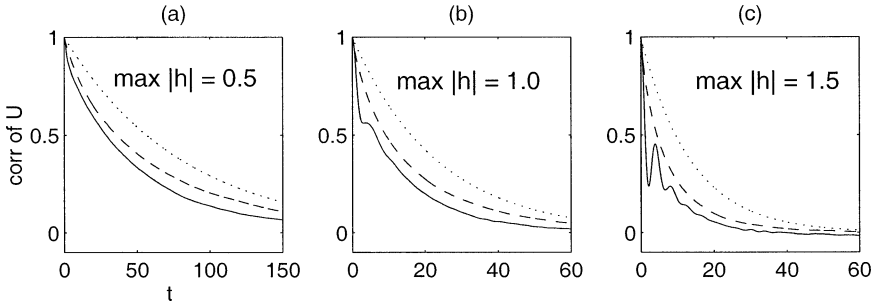

FIG. 13. Barotropic QG equation; comparison of the correlation function of U for three values of $\max|h| = 0.5, 1.0, 1.5$; DNS of the barotropic QG equation in (4.1) (solid line); nonlinear reduced stochastic model in (4.7) (dashed line); corresponding linear reduced stochastic model (dotted line).

system instead yields a PDF with two large peaks and two secondary peaks (see Figs. 7 and 8) that only weakly ''shadow'' this periodic orbit; in the example, only the correlation function of the variable x_1 (see Fig. 9), associated with the smaller peaks reflects any feature of the stable nonlinear oscillation in the projected nonlinear climate dynamics. Furthermore, the systematic procedure produces reduced stochastic equations for the two climate variables that reproduce all of the features in the climate dynamics of the deterministic equations in a quantitative fashion (Table 1, Figs. 7, 8, and 9). Key features of the reduced stochastic model, (3.4), are multiplicative noises and augmented nonlinearity produced through interaction with the unresolved variables that are predicted a priori by the systematic modeling strategy. Also note in this example that $x_1, x_2 \equiv 0, y_k, z_k \equiv 0$ is unstable for the deterministic system, yet arises as the climate mean state (Table 1). Furthermore, this zero state is in a basin of low probability in the PDF for the climate variables (Figs. 7 and 8) so the climate dynamics rarely visits the climatological mean state. This phenomenon is very similar to the one reported in Markov models for observational data for low-frequency behavior (Mo and Ghil 1988). These models also provide dramatic examples of the failure of standard regression fitting through Langevin-type linear models involving only linear equations with white noise forcing; in such a procedure, the correlation functions centered at the climatological mean state are fit by the procedure. Knowledge of only the mean state from Table 1 and the correlations in Figs. 9a–c strongly suggests such a linear Langevin regression fit, which has only Gaussian behavior; on the other hand, this approach must fail due to nonlinearity in the reduced dynamics; recall that both the PDF (Figs. 7 and 8) and the energy correlations, $K_2(t)$, exhibit strongly non-Gaussian behavior in the dynamics that is captured by the reduced stochastic model with nonlinear dynamics in (3.4).

Several interesting additional points also can be made for the deterministic system in section 3b with 101 degrees of freedom and simple multiple equilibria in the projected nonlinear climate dynamics. It is established there that both the strength of the coupling to the unresolved modes and the strength of nonlinear climate dynamics measured by λ in (3.5) determine whether the stable multiple equilibria are important (Fig. 10a) or relatively unimportant (Fig. 10c) in the deterministic dynamics. Furthermore, such features and transition regimes are captured by the predicted reduced one-dimensional nonlinear stochastic equation for the climate dynamics with additive noise in (3.7) including excellent a priori prediction of temporal correlations (Figs. 10 and 11) through all of the transition parameter regimes $\lambda = 0.15, 0.5, 1.2$. Since the role of multiple equilibria in predicted nonlinear climate dynamics in low-frequency variability is a controversial topic (Ghil and Robertson 2002), these examples and the reduced stochastic model quantify the issues surrounding the

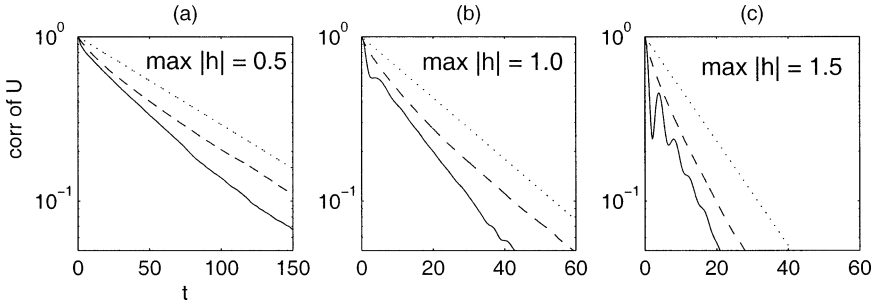

FIG. 14. Barotropic QG equation; same as in Fig. 13 on logarithmic scale.

importance of multiple equilibria in an unambiguous toy model. However, some of the controversy involves statistical issues with limited observational datasets, which cannot be addressed in the toy model. In more realistic systems, the climate variables interact with the unresolved variables through superposition of both types of triad interactions from the models in sections 2 and 3; the systematic stochastic modeling strategy predicts superposition of multiplicative noises, augmented nonlinearity, and additive noise in the general case [theorem (4.3) in MTV-2], and this should be useful for improved regression fitting strategies.

The systematic stochastic mode reduction strategies are applied in section 4 in an idealized context to the stochastic modeling of the effect of mountain torque on the angular momentum budget. Surprisingly, a new application of the stochastic modeling strategy is developed there that leads to a nonlinear stochastic equation for the large-scale mean. Furthermore, it is established there that such reduced nonlinear stochastic dynamics improve the predicted correlation functions significantly compared with the linear Langevin model.

The case study presented in section 4 involves the extreme situation of a single topographic Rossby mode interacting with the mean flow; this case is utilized here as a severe but simple test for the stochastic mode reduction strategy. Even the new nonlinear stochastic mode reduction procedure that accounts for the effect of the single topographic Rossby frequency through (4.5) and (4.8) cannot capture the oscillations in the correlation function for U evident in Figs. 12 and 13 for large topographic amplitudes when U is treated as the single climate variable. A systematic study by the authors of stochastic modeling for mountain torque with realistic large-scale multimode topography in spherical geometry with both quasigeostrophic and primitive equation models is in progress; the detailed results will be reported elsewhere.

Finally, there are several important issues for climate modeling that have not been addressed in the present work. The stochastic mode reduction strategy developed here assumes a partition into slower evolving climate variables and more rapidly evolving unresolved variables. How can such a partition be achieved in a complex climate model? The possibilities for developing such a partition range from utilizing a basis of empirical orthogonal functions in a suitable metric for the dynamics (Branstator 1995; Selten 1997), to a basis of optimally persistent patterns (DelSole 2001), to a basis of principal interaction patterns (Achatz et al. 1995), etc. Clearly, this is a central issue for the applicability of the stochastic-mode reduction procedures to realistic climate problems and warrants extensive research efforts. Other important issues for the use of stochastic-mode reduction in climate models involve the physical fidelity of the reduced models regarding changes in the external parameters of the climate as well as fidelity with the predictability characteristics of the climate variables. In particular, the validity of an accurate fluctuation–dissipation theorem (Leith 1975) for the reduced stochastic climate description is a fundamental problem. It was established in section 3 that the toy models introduced there exhibit substantial changes in the climate PDF that are captured by the stochastic reduced model. Thus, the models introduced here provide instructive examples for these central problems in climate research. The authors plan to report on these issues in the toy models in the near future.

Acknowledgments. The research of A. Majda is partially supported by NSF Grant DMS99-72865, ONR Grant N00014-96-1-0043, ARO Grant DAAD19-01-10810, as well as an NSF-CMG Grant DMS02-22133. I. Timofeyev was partially supported as a postdoctoral fellow through these grants. The research of E. Vanden-Eijnden is partially supported by NSF Grant DMS02-09959.

APPENDIX

Stochastic Mode Elimination

In this appendix, the reduced equation in (4.7) for the zonal mean flow U alone is obtained by mode elimination from the truncated barotropic equations in (4.4) under the stochastic consistency assumption in (4.6). For the reader's convenience, a heuristic, but strictly formal, derivation of (4.7) is first given. Next, the effective equation in (4.7) is reobtained in a systematic fashion by asymptotic analysis of Fokker–Planck operators, which can be made rigorous following Kurtz (1973). Notice that some difficulty arises with the heuristic derivation as concerns the interpretation of the multiplicative noise in (4.7); this problem is solved unambiguously by the systematic derivation of this equation. The interested reader is referred to Gardiner (1985, section 6.4) for a heuristic discussion of the mode elimination procedure on a simpler example with no problem of interpretation of the noise.

The truncated barotropic equations in (4.4) under the stochastic consistency assumption in (4.6) read

$$\frac{d\psi_{\mathbf{k}}}{dt} = ik_x H'_{\mathbf{k}} U - \gamma_{\mathbf{k}}(U)\psi_{\mathbf{k}} + \sigma_{\mathbf{k}}\dot{W}_{\mathbf{k}},$$

$$\frac{dU}{dt} = 2\ \mathrm{Im} \sum_{\mathbf{k}} k_x H'_{\mathbf{k}} \psi_{\mathbf{k}}, \tag{A.1}$$

where

$$\gamma_{\mathbf{k}}(U) = \gamma_{\mathbf{k}} + i\omega_{\mathbf{k}}(U), \quad \text{with}$$

$$\omega_{\mathbf{k}}(U) = \Omega'_{\mathbf{k}} + \frac{k_x}{\sqrt{\alpha\mu}} U. \tag{A.2}$$

The basic requirement to eliminate the unresolved modes, $\psi_{\mathbf{k}}$, from (A.1) is that these modes are so fast that they adjust themselves quasi-instantaneously to the value of the slow mode, U, whose evolution is sought. For (A.1) this adiabatic adjustment arises provided that

$\gamma_{\mathbf{k}}(U)$ is large enough; when this is the case, the second equation for $\psi_{\mathbf{k}}$ in (A.1) can be solved with U being kept frozen at its given value:

$$\psi_{\mathbf{k}}(t) \approx \psi_{\mathbf{k}}(0)\exp[\gamma_{\mathbf{k}}(U)t] + ik_x H'_{\mathbf{k}} U\int_0^t \exp[-\gamma_{\mathbf{k}}(U)s]\,ds + \sigma_{\mathbf{k}}\int_0^t \exp[-\gamma_{\mathbf{k}}(U)(t-s)]\dot{W}_{\mathbf{k}}(s)\,ds. \quad \text{(A.3)}$$

For time such that $\gamma_{\mathbf{k}}(U)t \gg 1$, the first term in this expression becomes negligible [i.e., the memory of the initial condition $\psi_{\mathbf{k}}(0)$ is lost], and the lower limit in the integrals can be pushed back to $-\infty$ without introducing any significant error. Therefore,

$$\psi_{\mathbf{k}}(t) \approx i\frac{k_x H'_{\mathbf{k}} U}{\gamma_{\mathbf{k}}(U)} + \sigma_{\mathbf{k}}\int_{-\infty}^t \exp[-\gamma_{\mathbf{k}}(U)(t-s)]\dot{W}_{\mathbf{k}}(s)\,ds, \quad \text{(A.4)}$$

and inserting this expression in the first equation for U in (A.1) leads after some manipulations to

$$\frac{dU}{dt} = -\gamma(U)U + \sqrt{2\gamma(U)}\xi(t). \quad \text{(A.5)}$$

Here the nonlinear damping factor $\gamma(U)$ is precisely the one given in (4.8), and $\xi(t)$ has been defined as

$$\xi(t) = \sqrt{\frac{2}{\gamma(U)}}\,\mathrm{Im}\sum_{\mathbf{k}} k_x H'_{\mathbf{k}}\sigma_{\mathbf{k}} \times \int_{-\infty}^t \exp[-\gamma_{\mathbf{k}}(U)(t-s)]\dot{W}_{\mathbf{k}}(s)\,ds. \quad \text{(A.6)}$$

Therefore, (A.5) is identical with (4.7) provided it can be shown that

$$\sqrt{2\gamma(U)}\xi(t) \approx \gamma'(U) + \sqrt{2\gamma(U)}\dot{W}, \quad \text{(A.7)}$$

in suitable limit. Establishing (A.7) requires to show that $\xi(t)$ is approximately delta correlated in time, and that the Fokker–Planck operator associated with this noise term has to be written is self-adjoint form [see (A.23) below]; the second requirement is what gives rise to the second term at the right-hand side of (A.7) that is in fact a noise-induced drift term, similar to the one which is obtained when a Stratonovich stochastic differential equation is rewritten in Itô's form. The white noise nature of $\xi(t)$ is rather straightforward to establish, as shown next. However, the second property for the Fokker–Planck operator is more subtle and cannot be obtained within the heuristic derivation; this property will be established afterwards in the systematic derivation of (4.4).

To establish the white noise nature of $\xi(t)$ heuristically, the autocorrelation function of this noise is computed and shown to be delta correlated in time. Using $\langle \dot{W}_{\mathbf{k}}(t)\dot{W}^*_{\mathbf{k}'}(t')\rangle = \delta(t-t')\delta_{\mathbf{k},\mathbf{k}'}$ it can be checked after a tedious but straightforward calculation that

$$\langle \xi(t)\xi(t')\rangle = \frac{1}{\gamma(U)}\sum_{\mathbf{k}} k_x^2 (H'_{\mathbf{k}})^2\sigma_{\mathbf{k}}^2 \exp[-\gamma_{\mathbf{k}}|t-t'|] \times \cos[\omega_{\mathbf{k}}(U)(t-t')]. \quad \text{(A.8)}$$

Since

$$\exp(-\gamma_{\mathbf{k}}|t-t'|)\cos[\omega_{\mathbf{k}}(U)(t-t')] \approx \frac{1}{\gamma_{\mathbf{k}}^2 + \omega_{\mathbf{k}}^2(U)}\delta(t-t'), \quad \text{(A.9)}$$

as $\gamma_{\mathbf{k}} \to \infty$, it follows from (A.8) using $\sigma_{\mathbf{k}}^2 = \gamma_{\mathbf{k}}$ that

$$\langle \xi(t)\xi(t')\rangle \approx \delta(t-t') \quad \text{(A.10)}$$

in this limit; therefore, $\xi(t)$ in (A.5) is indeed approximately a white noise.

The reduced equation in (4.7) can be derived in more systematic fashion by manipulating the Fokker–Planck equation associated with the stochastic model in (A.1). First, it is necessary to make the separation of timescale apparent by introducing a tracer parameter ε and rewriting (A.1) as

$$\frac{d\psi_{\mathbf{k}}}{dt} = \frac{i}{\varepsilon}k_x H'_{\mathbf{k}} U - \frac{\gamma_{\mathbf{k}}(U)}{\varepsilon^2}\psi_{\mathbf{k}} + \frac{\sigma_{\mathbf{k}}}{\varepsilon}\dot{W}_{\mathbf{k}},$$
$$\frac{dU}{dt} = \frac{2}{\varepsilon}\,\mathrm{Im}\sum_{\mathbf{k}} k_x H'_{\mathbf{k}}\psi_{\mathbf{k}}. \quad \text{(A.11)}$$

The parameter ε must be thought of as a small parameter, which allows us to distinguish the relative amplitude of the various terms in (A.11). Note that it has been assumed in (A.11) that all the terms entering $\gamma_{\mathbf{k}}(U)\psi_{\mathbf{k}}$–that is, the nonlinear interaction term $ik_x(\alpha\mu)^{-1/2}U\psi_{\mathbf{k}}$, the oscillatory term $i\Omega'_{\mathbf{k}}\psi_{\mathbf{k}}$, and the damping term $\gamma_{\mathbf{k}}\psi_{\mathbf{k}}$–are large and of the same order, ε^{-2}; this assumption must be checked a posteriori and, in the present case, leads indeed to results for the reduced equation that are consistent with the direct numerical simulation of the original equations in (4.4). The Fokker–Planck equation associated with (A.11) is

$$\frac{\partial f}{\partial t} = \frac{1}{\varepsilon}\mathcal{L}_1 f + \frac{1}{\varepsilon^2}\mathcal{L}_2 f, \quad \text{(A.12)}$$

where $\mathcal{L}_1$, $\mathcal{L}_2$ are the operators

$$\mathcal{L}_1 = 2\,\mathrm{Im}\sum_{\mathbf{k}} k_x H'_{\mathbf{k}}\psi_{\mathbf{k}}\frac{\partial}{\partial U} + \sum_{\mathbf{k}} ik_x H'_{\mathbf{k}} U\frac{\partial}{\partial\psi_{\mathbf{k}}}, \quad \text{(A.13)}$$

$$\mathcal{L}_2 = -\sum_{\mathbf{k}} \gamma_{\mathbf{k}}(U)\frac{\partial}{\partial\psi_{\mathbf{k}}} + \sum_{\mathbf{k}} \sigma_{\mathbf{k}}^2\frac{\partial^2}{\partial\psi_{\mathbf{k}}\partial\psi^*_{\mathbf{k}}}. \quad \text{(A.14)}$$

To take the limit as $\varepsilon \to 0$ in (A.12) and derive an equation for $f_0 = \lim_{\varepsilon\to 0} f$, the function f is formally expanded as $f = f_0 + \varepsilon f_1 + \varepsilon^2 f_2 + O(\varepsilon^3)$. Inserting

this expansion in (A.12) and regrouping the terms of order ε^{-2} leads to

$$\mathcal{L}_2 f_0 = 0, \tag{A.15}$$

which indicates that f_0 belongs to the null space of $\mathcal{L}_2$ or, equivalently, that $\mathbf{P}f_0 \equiv f_0$; here, $\mathbf{P}$ is the projection

$$(\mathbf{P}g)(U) = \int P_U(\psi) g(U, \psi)\, d\psi, \tag{A.16}$$

where g is a test function and $P_U(\psi)$ is the stationary PDF associated with the operator $\mathcal{L}_2$. Since $\mathcal{L}_2$ is the Ornstein–Uhlenbeck operator in $\psi_{\mathbf{k}}$, with U entering here as a parameter, $P_U(\psi)$ can be obtained explicitly (see e.g., appendix A of MTV-2) and is given by

$$P_U(\psi) = C \exp\left[- \sum_{\mathbf{k}} |\gamma_{\mathbf{k}}(U)|\, |\psi_{\mathbf{k}}|^2 / \sigma_{\mathbf{k}}^2 \right], \tag{A.17}$$

where C is a normalization constant. Next, regrouping the terms of order ε^{-1} in (A.12) with $f = f_0 + \varepsilon f_1 + \varepsilon^2 f_2 + \mathcal{O}(\varepsilon^3)$ leads to

$$\mathcal{L}_2 f_1 = -\mathcal{L}_1 f_0. \tag{A.18}$$

This equation has a solution only if the left-hand side belongs to the range of $\mathcal{L}_2$, which requires that $\mathbf{P}\mathcal{L}_1 f_0 = 0$; it can be checked that this condition is automatically satisfied in the present case. Therefore, the solution of (A.18) is

$$f_1 = -\mathcal{L}_2^{-1}\mathcal{L}_1 f_0. \tag{A.19}$$

Finally regrouping the terms of order 1 in (A.12) and using (A.19) gives

$$\mathcal{L}_2 f_2 = \frac{\partial f_0}{\partial t} + \mathcal{L}_1 \mathcal{L}_2^{-1} \mathcal{L}_1 f_0, \tag{A.20}$$

and the solvability condition for this equation, $\mathbf{P}$(right-hand side) = 0, leads to the desired equation for f_0

$$\frac{\partial f_0}{\partial t} = \mathcal{L} f_0, \qquad \mathcal{L} = -\mathbf{P}\mathcal{L}_1 \mathcal{L}_2^{-1} \mathcal{L}_1 \mathbf{P}. \tag{A.21}$$

The operator $\mathcal{L}_2^{-1}$ can be computed explicitly using again the fact that $\mathcal{L}_2$ is the Ornstein–Uhlenbeck operator in $\psi_{\mathbf{k}}$, with U entering as a parameter; the calculation is very similar to the one outlined in appendixes A and B of MTV-2, and the final result for $\mathcal{L}$ is

$$\mathcal{L} f_0 = -\gamma(U) U \frac{\partial f_0}{\partial U} + \gamma'(U) \frac{\partial f_0}{\partial U} + \gamma(U) \frac{\partial^2 f_0}{\partial U^2}, \tag{A.22}$$

with $\gamma(U)$ given by (4.8). It follows that the Itô equation associated with (A.21) is precisely (4.7). Notice that (A.22) shows that the second term at the right hand-side of (4.7) is indeed a noise-induced drift, as asserted before, since (A.23) can also be written as follows with the diffusive term in self-adjoint form:

$$\mathcal{L} f_0 = -\gamma(U) U \frac{\partial f_0}{\partial U} + \frac{\partial}{\partial U}\left[\gamma(U) \frac{\partial f_0}{\partial U} \right]. \tag{A.23}$$

REFERENCES

Achatz, U., and G. Branstator, 1999: A two-layer model with empirical linear corrections and reduced order for studies of internal climate variability. *J. Atmos. Sci.,* **56,** 3140–3160.

——, G. Schmitz, and K. M. Greisiger, 1995: Principal interaction patterns in baroclinic wave cycles. *J. Atmos. Sci.,* **52,** 3201–3213.

Branstator, G., 1995: Organization of storm track anomalies by recurring low-frequency circulation anomalies. *J. Atmos. Sci.,* **52,** 207–226.

——, and S. E. Haupt, 1998: An empirical model of barotropic atmospheric dynamics and its response to tropical forcing. *J. Climate,* **11,** 2645–2667.

Carnevale, G., and J. S. Frederiksen, 1987: Nonlinear stability and statistical mechanics for flow over topography. *J. Fluid Mech.,* **175,** 157–181.

Charney, J. G., and J. G. DeVore, 1979: Multiple flow equilibria in the atmosphere and blocking. *J. Atmos. Sci.,* **36,** 1205–1216.

DelSole, T., 2001: Optimally persistent patterns in time-varying fields. *J. Atmos. Sci.,* **58,** 1341–1356.

——, and B. F. Farrel, 1996: Quasi-linear equilibration of a thermally maintained, stochastically excited jet in a quasigeostrophic model. *J. Atmos. Sci.,* **53,** 1781–1797.

DeSwart, H. E., and J. Grasman, 1987: Effect of stochastic perturbations on a low-order spectral model of the atmospheric circulation. *Tellus,* **39A,** 10–24.

Egger, J., 2001: Master equations for climate parameter sets. *Climate Dyn.,* **18,** 169–177.

——, and K.-P. Hoinka, 2002: Covariance analysis of the global atmospheric axial angular momentum budget. *Mon. Wea. Rev.,* **130,** 1063–1070.

Frederiksen, J. S., M. R. Dix, and S. M. Kepert, 1996: Systematic energy errors and the tendency toward canonical equilibrium in atmospheric circulation models. *J. Atmos. Sci.,* **53,** 887–904.

Gardiner, C. W., 1985: *Handbook of Stochastic Methods,* Springer-Verlag, 442 pp.

Ghil, M., and S. Childress, 1987: *Topics in Geophysical Fluid Dynamics: Atmospheric Dynamics, Dynamo Theory, and Climate Dynamics.* Springer-Verlag, 485 pp.

——, and Robertson, A. W., 2002: ''Waves'' vs. ''Particles'' in the atmosphere's phases space: A pathway to long-range forecasting? *Proc. Natl. Acad. Sci. USA,* **99,** 2493–2500.

Gluhovsky, A., and C. Tong, 1999: The structure of energy conserving low-order models. *Phys. Fluids,* **11,** 334–343.

Griffies, S. M., and K. Bryan, 1997: A predictability study of simulated North Atlantic multidecadal variability. *Climate Dyn.,* **13,** 459–487.

Grote, M. A., A. J. Majda, and C. G. Ragazzo, 1998: Dynamic mean flow and small scale interaction through topographic stress. *J. Nonlinear Sci.,* **9,** 89–130.

Hasselmann, K., 1976: Stochastic climate models. Part I: Theory. *Tellus,* **28,** 473–485.

Itoh, H., and M. Kimoto, 1996: Multiple attractors and chaotic itinerancy in a quasigeostrophic model with realistic topography: Implications for weather regimes and low-frequency variability. *J. Atmos. Sci.,* **53,** 2217–2231.

Jin, F.-F., and M. Ghil, 1990: Intraseasonal oscillations in the extratropics: Hopf bifurcation and topographic instabilities. *J. Atmos. Sci.,* **47,** 3007–3022.

Khasminsky, R. Z., 1963: Principle of averaging for parabolic and elliptic differential equations and for Markov processes with small diffusion. *Theory Prob. Its Appl.,* **8,** 1–21.

Kimoto, M., and M. Ghil, 1993: Multiple flow regimes in the Northern Hemisphere winter. Part II: Sectorial regimes and preferred transitions. *J. Atmos. Sci.,* **50,** 2645–2673.

Kloeden, P. E., and E. Platen, 1995: *Numerical Solution of Stochastic Differential Equations.* Springer-Verlag, 632 pp.

Kurtz, T. G., 1973: A limit theorem for perturbed operators semi-

groups with applications to random evolution. *J. Funct. Anal.*, **12,** 55–67.

Legras, B., and M. Ghil, 1985: Persistent anomalies, blocking and variations in atmospheric predictability. *J. Atmos. Sci.,* **42,** 433–471.

Leith, C. E., 1975: Climate response and fluctuation dissipation. *J. Atmos. Sci.,* **32,** 2022–2025.

Lorenz, E. N., 1963: Deterministic non-periodic flow. *J. Atmos. Sci.,* **20,** 130–141.

Majda, A., and I. Timofeyev, 2000: Remarkable statistical behavior for truncated Burgers–Hopf dynamics. *Proc. Natl. Acad. Sci. USA,* **97,** 12 413–12 417.

——, ——, and E. Vanden-Eijnden, 1999: Models for stochastic climate prediction. *Proc. Natl. Acad. Sci. USA,* **96,** 14 687–14 691.

——, ——, and ——, 2001: A mathematical framework for stochastic climate models. *Commun. Pure Appl. Math.,* **54,** 891–974.

——, ——, and ——, 2002: A priori tests of a stochastic mode reduction strategy. *Physica D,* **170,** 206–252.

Marcus, S. L., M. Ghil, and J. O. Dickey, 1994: The extratropical 40-day oscillation in the UCLA general circulation model. Part I: Atmospheric angular momentum. *J. Atmos. Sci.,* **51,** 1431–1446.

——, ——, and ——, 1996: The extratropical 40-day oscillation in the UCLA general circulation model. Part II: Spatial structure. *J. Atmos. Sci.,* **53,** 1993–2014.

Mo, K.-C., and M. Ghil, 1988: Cluster analysis of multiple planetary flow regimes. *J. Geophys. Res.,* **93D,** 10 927–10 952.

Newman, M., P. Sardeshmukh, and C. Penland, 1997: Stochastic forcing of the wintertime extratropical flow. *J. Atmos. Sci.,* **54,** 435–455.

Obukhov, A. M., and F. V. Dolzhansky, 1975: On simple models for simulation of nonlinear processes in convection and turbulence. *Geophys. Fluid Dyn.,* **6,** 195–211.

Selten, F. M., 1997: A statistical closure of a low-order barotropic model. *J. Atmos. Sci.,* **54,** 1085–1093.

Trenberth, K. E., G. Branstator, D. Karoly, A. Kumar, N.-C. Lau, and C. Ropelewski, 1998: Progress during TOGA in understanding and modeling global teleconnections associated with tropical sea surface temperature. *J. Geophys. Res.,* **103,** 14 291–14 324.

Vautard, R., and B. Legras, 1988: On the source of midlatitude low-frequency variability. Part II: Nonlinear equilibration of weather regimes. *J. Atmos. Sci.,* **45,** 2845–2867.

Weickmann, K. M., W. Robinson, and C. Penland, 2000: Stochastic and oscillatory forcing of global atmospheric angular momentum. *J. Geophys. Res.,* **105,** 15 543–15 557.

Whitaker, J. A., and P. D. Sardeshmukh, 1998: A linear theory of extratropical synoptic eddy statistics. *J. Atmos. Sci.,* **55,** 237–258.